Available online at www.sciencedirect.com

ScienceDirect

Advances in Space Research xxx (xxxx) xxx

ADVANCES IN SPACE RESEARCH (a COSPAR publication)

www.elsevier.com/locate/asr

Geomechanical properties of lunar regolith simulants LHS-1 and LMS-1

Jared M. Long-Fox *, Zoe A. Landsman, Parks B. Easter, Catherine A. Millwater Daniel T. Britt

The University of Central Florida, Department of Physics, 4111 Libra Drive, Physical, Sciences Bldg. 430, Orlando, FL 32816, United States

Received 6 October 2022; received in revised form 21 January 2023; accepted 21 February 2023

Abstract

The geomechanical properties of mineralogically accurate lunar regolith simulants LHS-1 and LMS-1 are quantified and compared to published properties of lunar highlands and mare regolith, respectively, as well as to previously developed lunar simulants. Properties investigated include mineralogical and chemical composition, particle size distribution, density, shear strength, angle of repose, mass flow rates, and abrasivity. Results of data collection and analysis show that LHS-1 and LMS-1 are appropriate analogs for lunar regolith in terrestrial studies in the absence of returned lunar regolith and are preferable to non-mineralogically accurate simulants. Due to the mineralogy-based design philosophy, LHS-1 and LMS-1 naturally provide a good approximation of lunar regolith geochemistry and geomechanics that is suitable for studies in resource evaluation, acquisition, and extraction, mobility and optics, infrastructure development, and remote sensing.

Keywords: Moon; Regolith Simulants; ISRU; Geomechanics; Geotechnical engineering; Physical properties

1. Introduction

Governments, industry, and academic institutions are interested in establishing long-term human settlements on the lunar surface. The United States National Aeronautics and Space Administration (NASA) Artemis program and several other agencies intend to return humans to the Moon and plan to set up bases near the lunar south pole with exploration efforts aimed to cover the entire lunar surface. This interest in lunar exploration and infrastructure development drives the need for relevant materials to test technologies intended to be deployed on the lunar surface, but there are not sufficient amounts of returned lunar regolith samples available for bulk testing, as aliquots of only a few grams of returned regolith are given and most geomechanical tests require high sample masses. This means that the study of methods, development of technologies, and planning for long-term human presence on the Moon requires the use of high-fidelity lunar regolith simulants. Simulants serve as analogs for lunar regolith in the development and testing of hardware that will operate on the lunar surface, *in situ* manufacturing processes, and in scientific studies. The necessity of mineralogical accuracy is known to be important in many terrestrial studies regolith processing applications such as molten regolith electrolysis (MRE), sintering and additive manufacturing, and volatile extraction, but is also key in studies sensitive to the mechanical properties of the regolith. Most lunar simulants to date (e.g., JSC-1, BP-1, GRC-1, GRC-3) have disregarded mineralogic accuracy in favor of unnatural calibrations of bulk material properties of mineralogically

* Corresponding author.
E-mail address: jared.long-fox@ucf.edu (J.M. Long-Fox).

https://doi.org/10.1016/j.asr.2023.02.034
0273-1177/

inaccurate (and hence geomechanically inaccurate) materials by altering composition and particle size distributions until the desired physical properties are attained rather than letting the physical properties be driven by natural density and geometry of the mineral constituents.

As part of the NASA Solar System Research Virtual Institute (SSERVI) Center for Lunar and Asteroid Surface Science (CLASS), Cannon and Britt (2019) developed the Exolith Lab LHS-1 lunar highlands simulant (Fig. 1) and LMS-1 lunar mare simulant (Fig. 2) formulations (Table 1) with the goal of mineralogical fidelity. LHS-1 and LMS-1 use the well-characterized and relatively pristine lunar samples 67461 (Apollo 16, highlands origin) and 24999 (Luna 24, mare origin) as the mineralogical references for LHS-1 and LMS-1, respectively; the modal mineralogy for these samples (Simon et al., 1981) are shown in Table 2. LHS-1 and LMS-1 were created to simulate the geomechanical and geochemical properties of their respective lunar terranes by means of accurate mineralogy and reproducing lunar sample particle size distributions and shapes via percussive crushing methods. This work details the geomechanical properties of LHS-1 and LMS-1 to serve as standard reference materials for the lunar science and engineering communities to leverage in order to study, model, validate, and verify technologies for use on the lunar surface. Properties of LHS-1 and LMS-1 studied here include particle size distribution, density, shear strength, angle of repose, mass flow rates, and abrasivity.

2. Methods

2.1. Particle size

Exolith Lab controls for particle size at the process level, aiming to replicate the particle size distribution of the < 1 mm size fraction of the lunar regolith observed in returned samples in the Lunar Soils Grain Size Catalog (Graf, 1993). For the materials processed in-house at Exolith Lab, a series of rock crushers fitted with screens to remove the < 1 mm fraction are used. These percussive crushers naturally produce an approximate power law distribution of particle sizes and are intended to mimic the impact and gardening processes that form the lunar regolith through geologic time. For materials that arrive pre-crushed, Exolith Lab conducts particle size analysis using both sieves and a CILAS 1190 laser diffraction particle size analyzer (Orleans, France; https://www.particle-size.com). If needed, these feedstocks are sieved to produce the correct size distributions which are regularly verified using laser diffraction particle size analysis. The CILAS 1190 laser diffraction particle size analyzer can detect particles ranging from 0.04 μm to 2500 μm and is operated it in liquid dispersion mode with deionized (DI) water as the dispersing agent. The material to be tested is added to a vibrating dispersal cell, which is mechanically pumped into a measurement cell. There, lasers with wavelengths of 640 nm and 830 nm are allowed to strike incident upon the suspended particles in the measurement cell, and the particles diffract the light onto a detector. The CILAS Size Expert software pipeline (Orleans, France; https://www.particle-size.com) is used to analyze this pattern and compute the distribution of particle sizes of 5 random samples of LHS-1 and LMS-1. These five particle size distributions are averaged and the 95% confidence interval for each size bin is calculated and then compared to returned lunar samples identified as "Key Soils" by the Lunar Soils Characterization Consortium with data from the Lunar Soils Grain Size Catalog by Graf (1993).

Fig. 1. Exolith Lab lunar highlands simulant LHS-1.

Fig. 2. Exolith Lab lunar mare simulant LMS-1.

Table 1
Mineralogical compositions of LHS-1 and LMS-1 lunar regolith simulants.

Component	LHS-1 (wt.%)	LMS-1 (wt.%)
Anorthosite	74.4	19.8
Glass-rich basalt	24.7	32.0
Ilmenite	0.4	4.3
Olivine	0.2	11.1
Pyroxene	0.3	32.8

Please cite this article as: J. M. Long-Fox, Z. A. Landsman, P. B. Easter et al., Geomechanical properties of lunar regolith simulants LHS-1 and LMS-1, Advances in Space Research, https://doi.org/10.1016/j.asr.2023.02.034

Table 2
Modal mineralogy of reference samples 67461 and 24999 (1000–90 μm) from Simon et al. (1981) based on 189 and 634 points, respectively.

		67461 (Apollo 16, Highlands)	24999 (Luna 24, Mare)
Lithic Fragments	Mare Component		
	Mare basalts	0.5	6.9
	Highlands Component		
	ANT	21.7	3.5
	LMB	30.7	0.5
	Feldspathic Basalt	1.6	1.4
	RNB/POIK	7.9	2.2
Fused Soil Component	DMB	11.1	10.6
	Agglutinate	8.5	16.6
Mineral Fragments	Mafic	0.5	40.2
	Plagioclase	12.2	10.6
	Opaque	1.1	0.2
Glass Fragments	Orange/Black	0.5	–
	Yellow/Green	–	0.9
	Brown	–	0.2
	Clear	–	0.6
Miscellaneous	Devitrified Glass	3.2	5.4
	Others	0.5	0.3

2.2. Minimum, bulk Uncompressed, Maximum, and relative densities

The minimum density (ρ_{min}) of a granular material is the density of the material when the grains are packed in the loosest possible arrangement. The unconsolidated, low-density surficial lunar regolith is the first portion of the lunar surface that rovers and astronauts will encounter and are the most easily lofted, presenting danger to electronics, mechanical components, and human safety. The minimum density is a relatively unstable packing arrangement and represents the state at which a material is able to consolidate and deform the most under load or mechanical agitation, and unstable materials pose risk to structures and foundations constructed from and upon the material. The minimum density of mineralogically accurate simulants used for ground-based studies involving systems designed to interact with lunar regolith needs to be properly quantified to better inform on the range of densities that equipment and personnel may encounter during lunar operations. The minimum density of LHS-1 and LMS-1 was measured using a procedure conformal to ASTM D4254 (ASTM, 2016) as the mean of the mass-to-volume ratio of thirty known masses of simulant (100 ± 5 g) after gentle inversion in a 100 mL graduated cylinder with 1 mL resolution.

The bulk uncompressed density (ρ_b) is the "nominal" density of a material under unconfined, unagitated conditions. Since the bulk density is regarded as the typical density of granular materials, it is a key parameter in lunar ISRU and infrastructure development studies. Improper characterization of the uncompressed bulk density of lunar ISRU feedstock and building materials will result in suboptimal performance and introduce risk to equipment and personnel. Terrestrial studies that develop lunar systems will need to have good constraints on the bulk density of the simulant being used as well as use a mineralogically accurate simulant that naturally replicates the grain packing and grain density of lunar regolith. Discrepancies between results from laboratory testing with poorly characterized or inaccurate simulants and during operations on the lunar surface will impact efficiency and safety. The bulk uncompressed density of LHS-1 and LMS-1 was measured following ASTM D7481 (ASTM, 2018) where the bulk density is taken as the mean of 30 vol measurements of samples with masses of 100 ± 5 g after being poured from a funnel into a 100 mL graduated cylinder with 1 mL resolution.

The maximum density (ρ_{max}) of a granular geologic material represents the most dense packing of mineral grains possible. Constraints on maximum density of lunar regolith and appropriate analogs are critical for lunar system development because the strength of the material is highest at the maximum density, and thus serves as an upper limit to define operating conditions for probe instrumentation, roadway construction, landing pad development, and structure foundations. Mineralogically inaccurate simulants will not reproduce the maximum density of lunar regolith due to the differing mineralogic composition and grain geometries, rendering terrestrial studies performed with inappropriate simulants invalid and putting equipment and people at risk when the laboratory-developed methodologies are put to use on the Moon. The maximum density of LHS-1 and LMS-1 was measured by mechanically tapping 30 independent samples of 100 ± 5 g of simulant in a 100 mL graduated cylinder (1 mL resolution) until no further volume change is observed, and the final volume is recorded.

By using the minimum and maximum densities of lunar regolith and relevant simulants, it is possible to calculate the relative density (ρ_R) of a regolith sample. Relative density is not an absolute measure of density, but instead scales

Please cite this article as: J. M. Long-Fox, Z. A. Landsman, P. B. Easter et al., Geomechanical properties of lunar regolith simulants LHS-1 and LMS-1, Advances in Space Research, https://doi.org/10.1016/j.asr.2023.02.034

density as a percentage between minimum density (0% relative density) and maximum density (100% relative density) (ASTM, 2016). Relative density is one of the key parameters used to characterize the strength and stiffness *in situ* lunar regolith (Carrier et al., 1991) during exploration activities and ISRU activities. Following ASTM D4253 (ASTM, 2016) and ASTM D4254 (ASTM, 2016), relative density is calculated as:

$$\rho_R = \left(\frac{\rho_{max}}{\rho} \times \frac{\rho - \rho_{min}}{\rho_{max} - \rho_{min}}\right) \times 100\% \quad (1)$$

where ρ is the density of the sample being analyzed.

2.3. Shear strength

Shear strength (σ_s), and it's Mohr-Coulomb parameters of cohesion (c) and angle of internal friction (ϕ) are common characterizations of the strength of geologic materials. To quantify the shear strength of LHS-1 and LMS-1 in consolidated and drained conditions, a direct shear testing procedure that conforms to ASTM D3080 (ASTM, 2011) using custom hardware (Fig. 3) was developed.

In this procedure, a known mass of simulant is sheared in the known volume of the low-mass polycarbonate direct shear box with interior horizontal dimensions of 10.17 cm × 10.17 cm. Polycarbonate was chosen as the construction material for the custom direct shear testing equipment to ensure that negligible force is required to overcome friction between the top and bottom portions of the direct shear box during displacement. While loading the sample into the direct shear box, the simulant is gently agitated to encourage natural settling to typical densities observed during handling and other manipulations of the simulants. Once the simulant sample is loaded flush with the top of the direct shear box, another low-mass polycarbonate box (slightly smaller than the direct shear box) with a known mass of stacked, cut-to-size 6061 aluminum plates is placed on top of the simulant, while avoiding contact with the direct shear box, to prescribe a known normal load (σ_n) throughout the sample. The simulant is then sheared by displacing the upper portion of the simulant-filled shear box parallel to the plane of failure at a rate of 8 mm/s using an HP-500 digital push- pull force gauge (resolution of 0.1 N, ~0.01 kPa) connected to an Actuonix L16-R miniature linear servo that is driven by an Arduino UNO R3 microcontroller. 5 samples of shear force at failure are taken at seven normal loads (0.098, 0.193, 0.288, 0.383, 0.478, 0.573, and 0.668 kPa), giving a total of 35 measurements of shear force at failure that are subsequently converted to shear stress at failure (shear strength) based on the known area of the sheared simulant sample. This sampling strategy was selected to provide a wide range of normal force values and corresponding shear strengths to provide a statistically valid number of samples and characterize uncertainty in measurements at each normal load as well as in the overall Mohr-Coulomb linear fit (Eq. (2)).The relationship between measured shear strength and applied normal load is analyzed via linear regression under the assumptions of the Mohr-Coulomb Failure Criterion

$$\sigma_s = \sigma_n \tan\phi + c \quad (2)$$

This linear regression provides estimates of the best-fit c (intercept) and ϕ (arctangent of the slope), and 95% confidence intervals are calculated. The mass and volume of each direct shear sample are recorded during data collection, which allows for a quantitative estimate of the bulk density (ρ_b) of the simulant during direct shear testing of each simulant with 95% confidence intervals.

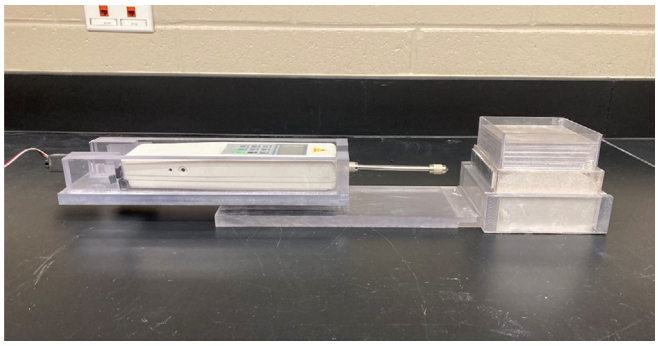

Fig. 3. Direct shear hardware including the direct shear box, normal force box, and aluminum plates to prescribe the normal load throughout the simulant during testing.

2.4. Angle of repose and slope failure

The angle of repose of a granular material is the steepest angle from a horizontal plane that the material can reach without experiencing slope failure. If the angle of repose is exceeded, the slope fails in order to return to a more stable, lower angle slope. The slope angles of LHS-1 and LMS-1 before (angle of repose) and after slope failure were measured by following the methodology of Geldart et al. (2006), and hardware used in shown in Fig. 4.

Here, five trials of 500 g each of LHS-1 and LMS-1 was poured through a polycarbonate funnel with an outlet diameter of 30 mm and a wall angle of 30° onto an angled chute 1 cm below the bottom of the funnel that is vibrated by four microcontroller-driven 3 V DC coin-style vibration motors. Simulant flows off the angled chute and hits the vertical wall of the simulant catch, causing the simulant to gently fall 15.5 cm into a half-cone pile on the bottom, horizontal platform. As simulant falls off the chute and onto the simulant catch, the pile of simulant repeatedly builds up to its angle of repose, undergoes slope failure, and repeats this cycle until the flow of simulant ceases. Video data of the simulant mound throughout 5 samples of each simulant are recorded by a GoPro Hero 5 Black that is positioned normal to the simulant catch. A 2.54 cm grid backdrop is placed behind the simulant catch to serve as a visual scale and increase contrast of each simulant with a consistent background. Video data are ana-

Please cite this article as: J. M. Long-Fox, Z. A. Landsman, P. B. Easter et al., Geomechanical properties of lunar regolith simulants LHS-1 and LMS-1, Advances in Space Research, https://doi.org/10.1016/j.asr.2023.02.034

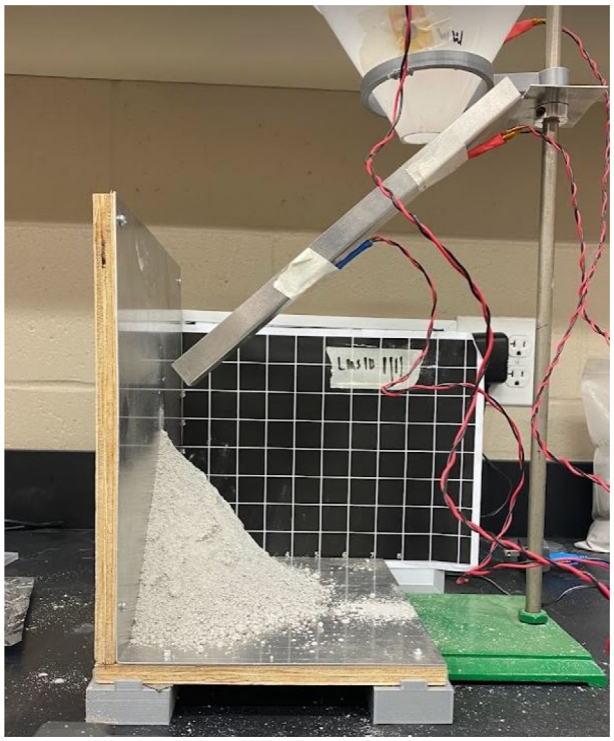

Fig. 4. Photograph of an angle of repose experiment showing the experimental setup including 30 mm funnel with 30° wall angle, chute, simulant catch, vibration motors, and contrasting 2.54 cm gridded backdrop.

lyzed using the Angle Tool in ImageJ (Schneider et al., 2012) to measure pre- and post-failure slope angles.

2.5. Mass flow rates

To quantify mass flow rates of LHS-1 and LMS-1, a method based on ASTM B964 (ASTM, 2016) was used. In this procedure, five independent samples of 500 ± 5 g of LHS-1 and LMS-1 were poured through polycarbonate funnels with identical 30° wall angles and outlet diameters of 25, 30, 35, 40, 45, 50, and 55 mm (all within ± 0.5 mm), resulting in a total of 35 mass flow rate samples for each simulant. Simulant flows out of a given funnel into a container resting on the weighing platform of an Intelligent Weighing Technology PBW-A 3200 laboratory balance that sends cumulative mass readings and elapsed time via serial communications to an external computer running a Python script that logs this serial data to a comma-delimited ASCII text file at a rate of 10 Hz. While simulant is flowing, the funnel is mechanically agitated by four 3 V DC coin-style vibration motors (driven by an Arduino UNO R3 microcontroller) to prevent cohesive arches from forming and stopping flow. The funnel is held 20 cm above the weighing platform by a custom, 3D printed mount that is attached to a standard laboratory rod and stand. Once the funnel and mount are positioned at the proper height above the weighing platform, the vibration motors are evenly spaced around the exterior of the funnel and the bottom of the funnel is blocked to prevent flow of material added to the funnel. Then, the simulant sample is gently poured into the funnel and, after confirming that the funnel is level and that the container to catch the simulant is in place on the weighing platform of the scale, the vibration motors are turned on, data logging is started, and the simulant is allowed to flow freely out of the funnel. Once all of the simulant has flowed out of the funnel and settled in the container on the laboratory balance, data collection is terminated, and the process is repeated as necessary for each sample of mass flow rates of each simulant out of each funnel.

The measured mass flow rates of LHS-1 and LMS-1 were analyzed via the relation proposed by Beverloo et al. (1961):

$$W = C\rho_b\sqrt{g}\left(D_o - Kd_p\right)^{5/2} \tag{3}$$

Where W is mass flow rate (g/min), ρ_b is bulk density of the simulant (g/cm^3), g is acceleration due to gravity (9.81 m/s^2) d_p is particle diameter, D_o is outlet diameter (cm), C is the dimensionless discharge parameter, and K is the dimensionless shape parameter. All terms except for C and K are known, so these are solved for in an adaptive Monte Carlo analysis where a random value for the nonlinear term K is generated and the measured mass flow rate data serve as optimization targets in a linear inversion to solve for the best-fit C given the guided random sample of K. For each sample of K (and its corresponding C value found via inversion), a forward model is calculated, the sum of squared errors (SSE) of the sample forward model is calculated. The adaptive Monte Carlo search works to find the best-fit (minimum SSE) K and C relative to observed data. The random value of K is drawn from a normal distribution with the current best-fit K value as the mean, which is initially set to 1.4, as given by Beverloo et al. (1961) and is updated every adaptation of 10,000 samples along with a narrowing of the K search distribution. The standard deviation (S_a) of each successive search adaptation shrinks according to the following cooling schedule:

$$S_a = S_0 e^{-a/2} \tag{4}$$

where the initial standard deviation $S_0 = 100$ and the analysis is run for a total of 10 adaptations (a = 0–9) of 10,000 samples each for a total of 100,000 total samples of C, K, and the corresponding SSE of each parameter combination at a final search precision of 1.11 for K. Uncertainties of the best-fit C and K values are quantified via F-test by using the ratio of the sample SSE to the best-fit SSE as the test (F) value to compare all sample model prediction and data variances. The resulting p-values for each set of C and K samples are used to determine the 95% confidence intervals for each parameter. This guided random search is used since LHS-1 and LMS-1 violate the Beverloo et al. (1961) assumptions of mono-sized particles of size greater than 0.5 mm, but the 5/2 power law has been found to

Please cite this article as: J. M. Long-Fox, Z. A. Landsman, P. B. Easter et al., Geomechanical properties of lunar regolith simulants LHS-1 and LMS-1, Advances in Space Research, https://doi.org/10.1016/j.asr.2023.02.034

be a good fit for quantifying granular flow in general (Mankoc et al., 2007). Since C and K are simply dimensionless scaling constants without apparent physical meaning (Mankoc et al., 2007), the same units given in Beverloo et al. (1961) are used for all terms in Eq. (3) to enable direct comparison between the general values of C and K recommended by Beverloo et al. (1961).

2.6. Abrasivity

Following the methods developed by Kobrick et al. (2010) and described in Landsman et al. (2021), Bud Labs (Rochester, NY, USA) conducted three-body abrasion testing of LHS-1 and LMS-1 using the proprietary Bud Labs Tribotester. Briefly, the abrasive material is placed below a dry rubber wheel with a diameter of 109 mm and width of 12.7 mm that spins at 30 RPM for 15 min for a total of 450 revolutions. The wheel forces the simulant against a test material with a force of 55 N. A simulants abrasivity is quantified by measuring the volume of the test material that was worn away by the simulant. Because of its relevance in aerospace engineering, standard 6061-T6 aluminum was the test material for this experiment. In addition to LHS-1 and LMS-1, two alternative lunar regolith simulants (JSC-1AF and NU-LHT-2 M) and two standard abrasives (50 μm alumina particles from Crystal Mark Inc. and 50–70 μm silica sand particles from Ottawa Sand) were also studied for comparison. These size fractions for the standard reference materials were used because they are similar to the mean particle sizes of LHS-1 and LMS-1. Bud Labs runs each test in triplicate to quantify uncertainty.

3. Results

3.1. Particle size

By taking 5 random, independent samples of LHS-1 and LMS-1 and analyzing their particle size distributions using the CILAS 1190 particle size analyzer and calculating 95% confidence intervals, it is determined that LHS-1 has a mean particle size of 87.95 ± 6.83 μm and median particle size of 61.78 ± 2.80 μm, and LMS-1 has a mean particle size of 85.65 ± 27.68 μm and a median particle size of 62.48 ± 8.02 μm. See Fig. 5 for graphs of the average of the 5 samples each of LHS-1 and LMS-1 particle size data plotted against lunar highlands and mare data, respectively, from the Lunar Soils Grain Size Catalog (Graf, 1993).

3.2. Minimum, bulk Uncompressed, Maximum, and relative density

See Table 3 for the results of testing for minimum, bulk uncompressed, and maximum densities of LHS-1 and LMS-1 in comparison to regolith from the lunar highlands and lunar mare from Carrier et al. (1991).

The relative density curves of LHS-1 and LMS-1 were calculated using Eq. (1) and are plotted alongside relative density curves from lunar highlands and mare regolith in Fig. 6. Data for the upper and lower bounds of regolith density measured for the highlands and mare used in these relative density calculations are the same as those given in Table 3.

3.3. Shear strength

Results from direct shear testing of LHS-1 and LMS-1 were analyzed via linear regression based on the Mohr-Coulomb Failure Criterion (Eq. (2)) and are shown graphically in Fig. 7 with the best-fit Mohr-Coulomb predictions and the corresponding 95% confidence intervals. The Mohr-Coulomb analysis of LHS-1 gives $c_{LHS} = 0.311 \pm 0.027$ kPa and $\phi_{LHS} = 31.49 \pm 3.67°$. The same regression analysis of LMS-1 gives $c_{LMS} = 0.393 \pm 0.035$ kPa and $\phi_{LMS} = 34.85 \pm 4.79°$.

3.4. Angle of repose and slope failure

Two slope failures were captured for each of the five angle of repose experiments, and the angle of repose (pre-failure angle) and angle after slope failure (post-failure

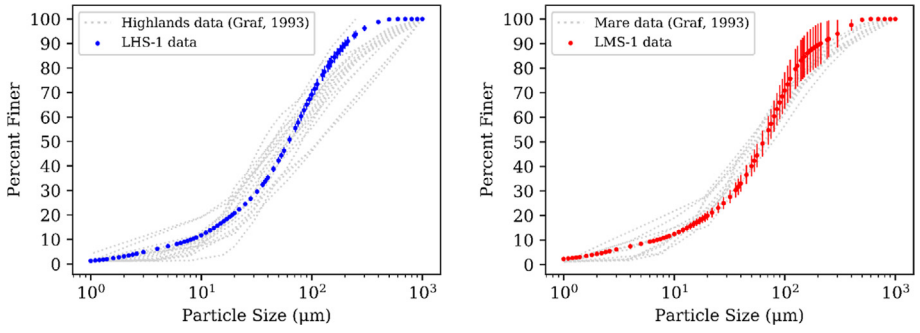

Fig. 5. Left: LHS-1 particle size data with error bars representing the 95% confidence interval plotted with particle size distributions of lunar highlands samples identified as "Key Soils" by the Lunar Soil Characterization Consortium from Graf (1993). Right: LMS-1 particle size data with error bars representing the 95% confidence interval plotted with particle size distributions of lunar mare samples identified as "Key Soils" by the Lunar Soil Characterization Consortium from Graf (1993).

Please cite this article as: J. M. Long-Fox, Z. A. Landsman, P. B. Easter et al., Geomechanical properties of lunar regolith simulants LHS-1 and LMS-1, Advances in Space Research, https://doi.org/10.1016/j.asr.2023.02.034

Table 3
Minimum, bulk uncompressed, and maximum densities of LHS-1 and LMS-1 with 95% confidence intervals and ranges of each measure of density of lunar highlands and mare regolith.

	LHS-1	LMS-1	Lunar Highlands	Lunar Mare
Minimum Density (ρ_{min}, g/cm^3)	1.27 ± 0.01	1.47 ± 0.03	1.1 – 1.2[a]	1.15 – 1.30[b]
Uncompressed Bulk Density (ρ_b, g/cm^3)	1.34 ± 0.03	1.54 ± 0.03	1.4 – 1.8[d]	1.55 – 1.90[b]
Maximum Density (ρ_{max}, g/cm^3)	1.86 ± 0.04	1.95 ± 0.06	1.7 – 1.8[a]	1.80[b] – 1.93[c]

[a]Luna 20 data from Carrier et al. (1991)
[b]Apollo 11 data from Carrier et al. (1991)
[c]Apollo 12 data from Carrier et al. (1991)
[d]Apollo 16 data from Mitchell et al. (1972)

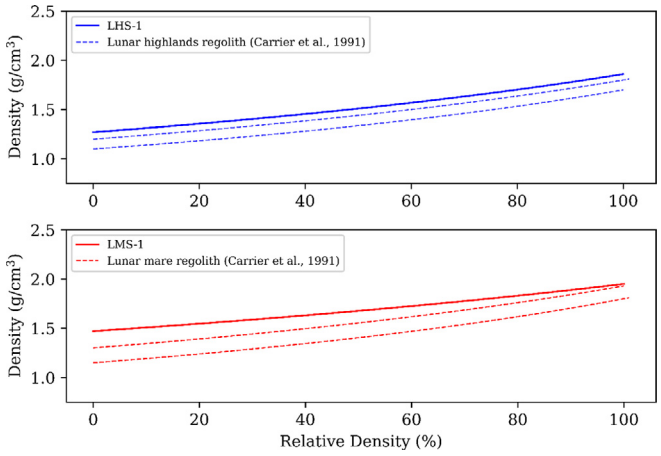

Fig. 6. Relative density plot for LHS-1 and lunar highlands regolith (top) and LMS-1 and lunar mare regolith (bottom). Lunar highlands and mare minimum and maximum density data used to construct the upper and lower bounds of regolith density are from Carrier et al. (1991). It is shown that the density profile of LHS-1 is a close match to that of lunar highlands regolith in terms of shape and magnitude and LMS-1 is a close match to lunar mare regolith at high relative densities.

angle) are given as averages of these angles with 95% uncertainties in Tables 4 and 5 for LHS-1 and LMS-1, respectively; an example image of the results of an angle of repose measurement after the experiment has ended given in Fig. 8. It is seen that the maximum pre-failure slope angle of LHS-1 is 47.5°, with an average of 41.2 ± 8.1°, and the maximum post-failure angle is 39.5° with an average of 30.9 ± 10.0°. The average change in slope from pre- to post-failure of LHS-1 is 10.3 ± 7.9° and the maximum change in slope was 17.1°. During these experiments, the maximum pre-failure slope angle of LMS-1 is 38.0° with an average of 37.5 ± 3.4°, the maximum post-failure angle was 32.0° with a mean of 28.0 ± 6.3°. The maximum change in slope angle after failure for LMS-1 was 11.9° and the mean change in slope of LMS-1 was 7.7 ± 7.4°.

3.5. Mass flow rates

Measuring the mass flow rates of LHS-1 and LMS-1, followed by a stochastic fitting routine to find the best-fit values of C and K from the Eq. (3) (Beverloo et al., 1961) yields results shown in Fig. 9 for LHS-1 and Fig. 10 for LMS-1. Fig. 9 shows the mass flow rate data along with the best-fit model for LHS-1 mass flow rates with $C = 31.45 \pm^{4.25}_{3.86}$ and $K = -23.63 \pm^{25.85}_{27.89}$ plotted in comparison to the standard Beverloo et al. (1961) parameter values of $K = 1.4$ and $C = 35$ as well as the estimated probability density functions of C and K for LHS-1 along with their 95% confidence intervals. Fig. 10 shows the mass flow rate data along with the best-fit model for LMS-1 mass flow rates with $C = 39.59 \pm^{4.42}_{4.11}$ and $K = -125.46 \pm^{26.04}_{27.95}$ plotted in comparison to the standard Beverloo et al. (1961) parameter values of $K = 1.4$ and $C = 35$ as well as the estimated probability density functions of C and K for LMS-1 along with their 95% confidence intervals.

3.6. Abrasivity

Using the methodology developed by Kobrick et al. (2010) and Landsman et al. (2021) for standard reference materials silica and alumina and previously developed lunar simulants JSC-1AF (the finest 20% fraction of JSC-1A) (McKay et al., 1994) and NU-LHT-2 M (Stoeser et al., 2010) are visually compared to LHS-1 and LMS-1 in Fig. 11 and quantitative results with 95% uncertainties are given in Table 6.

4. Discussion

4.1. Particle size

Particle size and particle size distribution greatly affect the mechanical, thermal, electrical, and volatile retention properties of a regolith and were ranked the first and second most important simulant properties, respectively, by the 2005 Lunar Simulant Workshop (Sibille et al., 2006). The particle size distribution of LHS-1 is in conformity with the particle size distributions of key lunar highlands regolith samples in the < 1000 μm size fraction (Fig. 5 left), and the particle size distribution of LMS-1 conforms to the size distributions of key lunar mare regolith samples in the < 1000 μm fraction (Fig. 5 right). It is seen that the per-

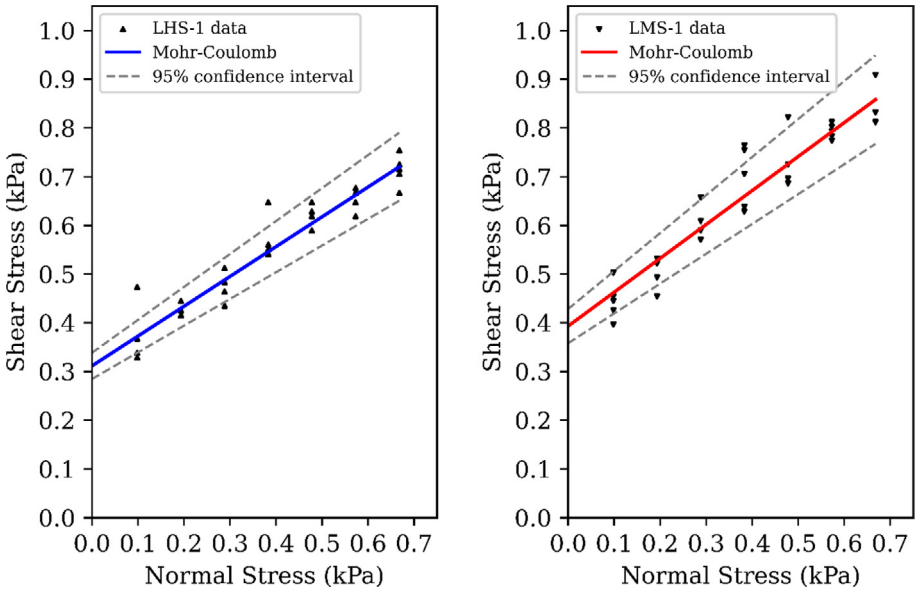

Fig. 7. Results of direct shear testing LHS-1 (left) with a density of 1.32 g/cm^3 (11.94% relative density) and LMS-1 (right) with a density of 1.65 g/cm^3 (44.32% relative density) with the respective best-fit Mohr-Coulomb predictions and corresponding 95% confidence intervals.

Table 4
Results of angle of repose and slope failure testing of LHS-1. Uncertainties given represent the 95% confidence interval.

	Pre-Failure Angle (°)	Post-Failure Angle (°)	Change in Slope (°)
Failure 1	45.0	37.8	7.2
	44.0	31.6	12.4
	40.2	27.5	12.7
	47.5	39.5	8.0
	42.0	33.7	8.3
Failure 2	40.1	23.0	17.1
	38.5	31.9	6.6
	33.0	27.1	5.9
	38.1	29.0	9.1
	43.7	27.5	16.2
Average	41.2 ± 8.1	30.9 ± 10.0	10.3 ± 7.9

Table 5
Results of angle of repose and slope failure testing of LMS-1. Uncertainties given represent the 95% confidence interval.

	Pre-Failure Angle (°)	Post-Failure Angle (°)	Change in Slope (°)
Failure 1	35.6	28.0	7.6
	34.7	27.1	7.6
	37.0	30.0	7.0
	37.5	23.5	14.0
	37.5	25.6	11.9
Failure 2	38.0	29.5	8.5
	33.0	23.0	10.0
	35.0	29.5	5.5
	35.0	32.0	3.0
	33.6	32.0	1.6
Average	37.5 ± 3.4	28.0 ± 6.3	7.7 ± 7.4

cussive crushing methods used to manufacture LHS-1 and LMS-1 result in consistent particle size distributions that match returned lunar regolith samples. The variability of particle sizes of LHS-1 is lower than that of LMS-1, and this is primarily attributed to the relatively more intensive in-house material processing of the LMS-1 material feedstock. The anorthosite in both LHS-1 and LMS-1 is purchased in bulk and already crushed to certain size ranges, which leaves the other major mineralogical phase of LHS-1 (basalt) and the minor phases (<1 wt% cumulative olivine, pyroxene, and ilmenite) to be crushed during in-house production of LHS-1. The feedstock for LMS-1,

Please cite this article as: J. M. Long-Fox, Z. A. Landsman, P. B. Easter et al., Geomechanical properties of lunar regolith simulants LHS-1 and LMS-1, Advances in Space Research, https://doi.org/10.1016/j.asr.2023.02.034

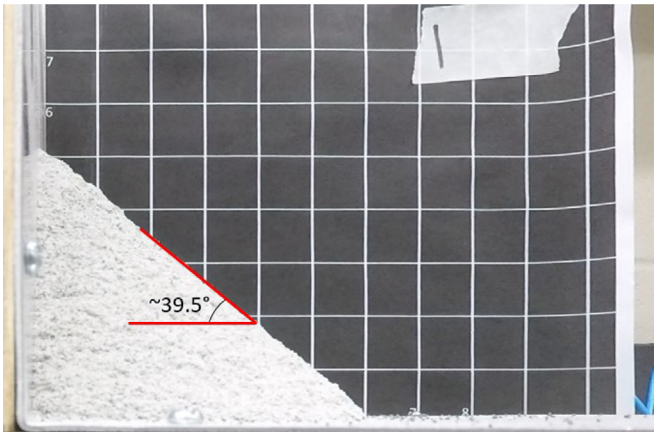

Fig. 8. Exemplary photograph of an angle of repose experiment on LHS-1 after simulant has stopped falling into the pile against a contrasting background grid of 2.54 cm squares.

which has a more diverse mineralogy than LHS-1, require more processing to achieve the desired particle size distributions, introducing some variability (similar to the natural variability seen in lunar regolith), but still allowing LMS-1 to serve as a high-fidelity, standard reference material for lunar mare regolith. Future studies should characterize the shape and surface morphology of lunar regolith simulants, as these affect geomechanical properties and volatile retention (Long-Fox et al., 2022).

4.2. Minimum, bulk Uncompressed, Maximum, and relative density

Previously developed simulants combined inaccurate mineral components to force the creation of a material with the desired density (e.g., Oravec et al., 2010), but LHS-1 and LMS-1 achieve a close fit to lunar highlands and mare regolith by leveraging the natural mineral grain densities,

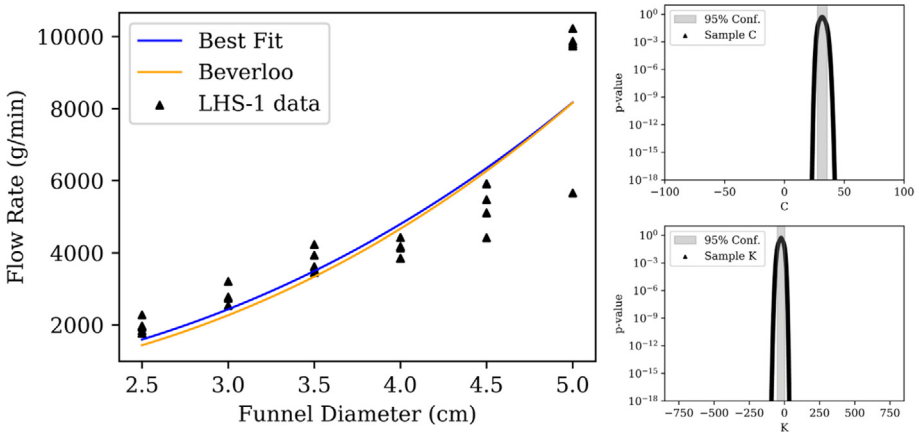

Fig. 9. Mass flow rates of LHS-1 plotted with the best-fit estimates of C (discharge parameter) and K (shape parameter) based on Beverloo et al. (1961) and the standard Beverloo model using the standard values for C (35) and K (1.4) as given by Beverloo et al. (1961) (left). Probability density functions estimated for the C (top right) and K (bottom right) parameters for LHS-1 where the grey shaded regions represent the 95% confidence interval.

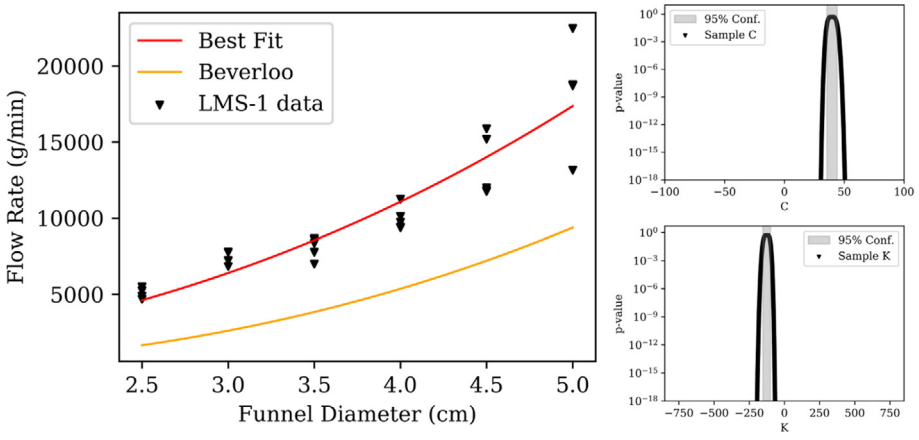

Fig. 10. Mass flow rates of LMS-1 plotted with the best-fit estimates of C (discharge parameter) and K (shape parameter) based on Beverloo et al. (1961) and the standard Beverloo model using the standard values for C (35) and K (1.4) as given by Beverloo et al. (1961) (left). Probability density functions estimated for the C (top right) and K (bottom right) parameters for LMS-1 where the grey shaded regions represent the 95% confidence interval.

Please cite this article as: J. M. Long-Fox, Z. A. Landsman, P. B. Easter et al., Geomechanical properties of lunar regolith simulants LHS-1 and LMS-1, Advances in Space Research, https://doi.org/10.1016/j.asr.2023.02.034

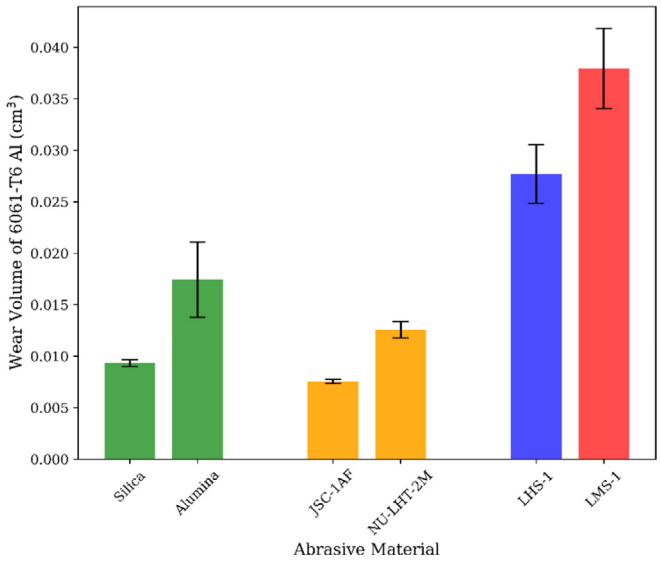

Fig. 11. Results of abrasion testing of standard reference materials (50–70 μm silica and 50 μm alumina particles) compared to previous lunar simulants (JSC-1AF and NU-LHT-2 M) and LHS-1 and LMS-1. Error bars represent 95% uncertainties.

Table 6
Abrasion testing results with 95% uncertainties for the silica (50–70 μm) and alumina (50 μm) as standard reference materials, previously developed lunar simulants JSC-1AF (McKay et al., 1994) and NU-LHT-2 M (Stoeser and Wilson, 2010), LHS-1, and LMS-1 (this study).

Material	Wear Volume of 6061-T6 Al (cm^3)
Silica	0.0093 ± 0.0003
Alumina	0.0174 ± 0.0037
JSC-1AF	0.0076 ± 0.0039
NU-LHT-2 M	0.0126 ± 0.0015
LHS-1	0.0277 ± 0.0029
LMS-1	0.0380 ± 0.0039

mineralogic proportions, and a lunar-like particle size distribution. The minimum density of LHS-1 is slightly higher than that of lunar highlands regolith, the mean bulk density is slightly lower, and the mean maximum density is slightly higher than lunar highlands materials, but the bulk and maximum density uncertainties overlap with lunar highlands measurements, as shown in Table 3. LHS-1 shows good alignment to the density profile of lunar highlands regolith (Fig. 6 top), which is owed to the high mineralogical accuracy of LHS-1. The average minimum density of LMS-1 is higher than that of lunar mare regolith, but the bulk and maximum density data collected from returned mare samples lie within confidence of the uncompressed bulk density and maximum densities of LMS-1.

During experiments, it was noted that LMS-1 takes less mechanical agitation to reach a higher relative density compared to LHS-1, so slight disturbances to the sample during experiments are more likely to disturb the fragile arrangement of particles at low densities and force a more stable, but more dense packing of particles and could explain the mismatch of LMS-1 and lunar mare regolith minimum densities. The less dense packing arrangements of LHS-1 were not as sensitive to slight disturbances from handling during experiments as LMS-1, attributed to the high anorthosite content which has grains with a high aspect ratio and may resist packing more than the mineralogically diverse LMS-1 with a greater variety of grain shapes that are able to fill in voids more completely. In personal communications with the Norwegian Geotechnical Institute (NGI), the minimum densities of LHS-1 and LMS-1 were measured to be ~ 10–20% greater than those measured here, the maximum density of LMS-1 was measured ~ 10% higher than this work, and the maximum density of LHS-1 was measured to be nearly the same as presented here (personal communication, Dylan Mikesell, NGI). The methods used to produce these minimum and maximum densities at NGI differed from those used here, indicating that a single, standardized testing procedure is necessary to properly define these parameters for regolith simulants.

4.3. Shear strength

Shear strength is a key characterization of the behavior of geologic materials. LHS-1 and LMS-1 are suitable analogs in terms of shear strength because the Mohr-Coulomb parameters of cohesion and angle of internal friction of LHS-1 and LMS-1 are both within bounds of the various estimates for lunar regolith given by Carrier et al. (1991) for both the Surveyor Model and Apollo Model best estimates. Previously developed, non-mineralogically accurate simulants such as GRC-3 (He et al., 2013), JSC-1A (McKay et al., 1994) and NU-LHT-2 M (Stoeser and Wilson, 2010) are generally created to mimic the shear strength of lunar regolith but do so without an accurate mineralogy, giving an unnatural calibration and sacrificing fidelity in other properties. Due to the lack of returned lunar samples available for bulk testing, very few laboratory studies of the shear strength of lunar regolith have been performed, and the studies that are published show wide variation in parameter estimates (Costes et al., 1970; Carrier et al., 1972). The density (absolute and relative) of regolith is related to its cohesion (Carrier et al., 1991), and the direct shear tests performed on LHS-1 and LMS-1 here were performed at different relative densities, but the tested densities are nominal densities observed when actively manipulating the simulants, so these estimates represent the shear strength of LHS-1 and LMS-1 at densities expected during laboratory testing. As previously stated, LMS-1 is more prone to settle into relatively dense packing arrangements compared to LHS-1, and as such, was tested at a higher relative density due to the nature of the simulants during handling. Due to the fragility of the less dense packing arrangements and the heavier mineralogy, it is not surprising that the cohesion for LMS-1 is higher than that of LHS-1. Ongoing work includes shear strength testing of LHS-1 and LMS-1 at different relative densities to charac-

Please cite this article as: J. M. Long-Fox, Z. A. Landsman, P. B. Easter et al., Geomechanical properties of lunar regolith simulants LHS-1 and LMS-1, Advances in Space Research, https://doi.org/10.1016/j.asr.2023.02.034

terize the relationship between shear strength, particle size, mineralogy, and relative density (Millwater et al., 2022).

4.4. Angle of repose and slope failure

The maximum pre-failure slope angle of LHS-1 was found to be 47.5°, and the maximum pre-failure angle of LMS-1 during experiments was 37.5°, both of which are near the (highly varied) published values for the angle of repose of lunar regolith (Carrier et al., 1991; Calle and Buhler, 2020). It should be noted that previous studies that performed angle of repose experiments on lunar regolith (e.g., Calle and Buhler, 2020) use less than ~ 20 g of regolith and non-standard test methods. This is an important consideration since the amount of material used is known to impact slope stability (Carrier et al., 1991) and this is being investigated to quantify slope stability of LHS-1 and LMS-1 as it scales with volume. Preliminary results show that at least 250 g of material is needed to get a consistent measure of angle of repose, indicating that tests run with less than 250 g are not comparable to what will be seen in bulk, *in situ* situations. Discrepancies and variations in slope stability during the experiment here may be caused by inconsistencies in the flow of simulant out of the funnel, onto the chute, and into the pile. Video data show slope failure occurring before the maximum angle is reached if there is a sudden, large influx of simulant and the dynamic force of the rapid addition to the pile causes slope failure prior to reaching the angle of repose. Efforts are ongoing to characterize the effect of variation of the rate at which simulant falls into the pile and to determine a relationship between pre- and post-slope failure angles as a function of mineralogy and particle size (Easter et al., 2022) as well as comparisons to other methodologies. As seen here (and expected to be seen on the lunar surface), the magnitude of slope failure, as well as the pre- and post-failure angles are highly variable, but on average are higher in LHS-1 than LMS-1. This difference is thought to be caused by the crystal habit of the dominant mineral in the lunar highlands, platy (high aspect ratio) anorthosite. Specifically, the mineralogy of LHS-1 is considered to enable greater slope stability than the more random assortment of mineral grain geometries in LMS-1, which is notably easier to pack and is less stable than LHS-1 at low densities. This does indicate fundamental differences in angle of repose between surfaces dominated by highlands mineralogies and those of mare mineralogies. This has direct implications for mobility, mission operations, and the design of regolith structures and berms and indicates that mineralogically inaccurate simulants are not suitable for general lunar geomechanics research and development.

4.5. Mass flow rates

The mass flow rates of LHS-1 and LMS-1, as a function of funnel outlet diameter, follow the 5/2 power law that is commonly suggested for the flow of granular materials (Beverloo et al., 1961; Mankoc et al., 2007), but the shape coefficients (K) are drastically different than the suggested value of 1.4. This is assumed to be a result of the extremely fine particles and wide particle size distribution of the simulants since the Beverloo et al. (1961) solution is only valid for mono-sized particles above 0.5 mm. The discharge coefficients (C) and corresponding uncertainties of LHS-1 and LMS-1 overlap with or are very near) the standard value of 35 recommended by Beverloo et al. (1961). This is attributed to the fact that the C parameter is related to density and gravitational acceleration, and the Beverloo et al. (1961) model was developed using various material densities (including sand) in ambient terrestrial conditions. The K parameter values for LHS-1 and LMS-1 have overlapping 95% confidence intervals, but the C value confidence intervals do not overlap. The difference in K values is attributed to mineralogy – the minerals in LHS-1 and LMS-1 have different crystal habits, so it is not a surprise that the K shape factor is significantly different. The similarity of the C values estimated for LHS-1 and LMS-1 is assumed to be a result of the similar particle size distributions of LHS-1 and LMS-1. Overall, the mass flow rates of LMS-1 are much higher than that of LHS-1, and the standard model of Beverloo et al. (1961) ($C = 35.0$, $K = 1.4$) underestimates the mass flow rates of LMS-1 but are a good match for LHS-1. The underestimation of LMS-1 mass flow rates is thought to be caused by the relatively high density of LMS-1 relative to the materials tested to develop the Beverloo et al. (1961) model. Work is ongoing to characterize the mass flow rates of LHS-1 and LMS-1 as a function of particle size and using alternative models such as that proposed by Mankoc et al. (2007). These results indicate that mass flow rates are sensitive to mineralogy and that operations on the lunar surface that deal with conveyance of regolith through hopper and funnel systems will need to be optimized to accommodate a wide range of granular flow rates.

4.6. Abrasivity

The hardness and grain geometry dominate the abrasive properties of geologic materials, and the lunar regolith is known to have high abrasivity that threaten astronauts and equipment during lunar operations (Rickman and Street, 2008; Fontes et al., 2022), so it is important for any simulants used in mechanical testing of equipment intended for use on the lunar surface appropriately replicate the abrasive properties of actual lunar regolith. Previously developed simulants with low mineralogical accuracy, such as JSC-1AF and NU-LHT-2 M, are shown to be as or less abrasive than standard silica, as shown in Fig. 11 and Table 6. The mineralogically accurate LHS-1 and LMS-1 are significantly more abrasive, at the 95% confidence level, than the standard silica and alumina as well as JSC-1A (McKay et al., 1994) and NU-LHT-2 M (Stoeser and Wilson, 2010) tested here. LMS-1 is seen to be significantly more abrasive than LHS-1 (and both

Please cite this article as: J. M. Long-Fox, Z. A. Landsman, P. B. Easter et al., Geomechanical properties of lunar regolith simulants LHS-1 and LMS-1, Advances in Space Research, https://doi.org/10.1016/j.asr.2023.02.034

LHS-1 and LMS-1 are more abrasive than the standard materials and other simulants tested), which is a function of the differences in mineralogy of these simulants. These results confirm that mineralogical accuracy is important in mechanical testing of lunar regolith simulants because the natural grain geometry and hardness of each mineral contributes to the overall abrasiveness.

5. Conclusions

The high fidelity of the LHS-1 and LMS-1 simulants is attributed to the mineralogy-based design philosophy behind their manufacture. Combined with an accurate particle size distribution, a material's mineralogy controls the geochemical as well as physical properties. Mineralogy, combined with an accurate particle size distribution, controls the density, packing arrangements, and grain geometry of the materials, hence impacting physical properties such as shear strength, angle of repose, material flow characteristics, abrasivity, and more. The properties of LHS-1 and LMS-1 investigated here are compared to published data of province-specific (highlands or mare) regolith data, as able, and are found to be good matches to returned regolith samples in terms of composition (Simon et al., 1981; Isachenkov et al., 2022) but also in terms of mechanical properties (Costes et al., 1970; Carrier et al., 1972; Carrier et al., 1991). Hence, LHS-1 and LMS-1 are well-suited for research and development projects that are sensitive to geochemistry and geomechanics including, but not limited to, into lunar ISRU, infrastructure development and remote sensing applications.

Declaration of Competing Interest

The authors declare that they have no known competing financial interests or personal relationships that could have appeared to influence the work reported in this paper.

Acknowledgements

This work was supported by NASA Cooperative Agreement 80NSSC19M0214 to the Center for Lunar and Asteroid Surface Science (CLASS) as part of the Solar System Exploration Research Virtual Institute (SSERVI). We gratefully acknowledge: Dr. Joe Donoghue, Dr. Kerri Donaldson Hanna, and Autumn Shackelford for training and access to the particle size analyzer; Dr. Ryan Kobrick and Bud Labs for their collaboration on abrasion testing; Dr. Clive Neal and Dr. Michael Lucas for critical discussions of lunar geology and interpretations as well as feedback on experiment designs.

References

ASTM Standard B964, 2016. Standard Test Methods for Flow Rate of Metal Powders Using the Carney Funnel, ASTM International, West Conshohocken, PA.

ASTM Standard D3080, 2011. Standard Test Method for Direct Shear Test of Soils Under Consolidated Drained Conditions, ASTM International, West Conshohocken, PA.

ASTM Standard D4253, 2016. Standard Test Methods for Maximum Index Density and Unit Weight of Soils Using a Vibratory Table, ASTM International, West Conshohocken, PA.

ASTM Standard D4254, 2016. Standard Test Methods for Minimum Index Density and Unit Weight of Soils and Calculation of Relative Density, ASTM International, West Conshohocken, PA.

ASTM Standard D7481, 2018. Standard Test Methods for Determining Loose and Tapped Bulk Densities of Powders using a Graduated Cylinder, ASTM International, West Conshohocken, PA.

Beverloo, W., Leniger, H., van de Velde, J., 1961. "The flow of granular solids through orifices. Chem. Eng. Sci. 15, 260–269. https://doi.org/10.1016/0009-2509(61)85030-6.

Calle, C.I., Buhler, C.R., 2020. Measurement of the Angle of Repose of Apollo 14 Lunar Sample 14163, Lunar Dust 2020 (LPI Contrib. No. 2141).

Cannon, K.M., Britt, D.T., 2019. Mineralogically Accurate Simulants for Lunar ISRU, and Strategic Regolith Processing. LPI Contributions 2152, 5002.

Carrier, W.D., Bromwell, L.G., Martin, R.T., 1972. Strength and Compressibility of Returned Lunar Soil. In: Proceedings of the 3rd Lunar Science Conference.

Carrier, W.D., Olhoeft, G.R., Mendell, W., 1991. Chapter 9: Physical Properties of the Lunar Surface, The Lunar Sourcebook. Cambridge University Press, Chapter 9.

Costes, N.C., Carrier, W.D., Mitchell, J.K., Scott, R.F., 1970. Apollo 11 Soil Mechanics Investigation. Science 167 (3918), 739–1471. https://doi.org/10.1126/science.167.3918.73.

Easter, P., Long-Fox, J., Landsman, Z., Metke, A., Britt, D., 2022. Comparing the Effects of Mineralogy and Particle Size Distribution on the Angle of Repose for Lunar Regolith Simulants. In: Proceedings of the 53rd Lunar and Planetary Science Conference, Houston, TX, USA.

Fontes, D., Mantovani, J.G., Metzger, P., 2022. Numerical estimations of lunar regolith trajectories and damage potential due to rocket plumes. Acta Astronaut. 195, 169–182. https://doi.org/10.1016/j.actaastro.2022.02.016.

Geldart, D., Abdullah, E., Hassanpour, A., Nwoke, L., Wouters, I., 2006. Characterization of powder flowability using measurement of angle of repose. China Particuol. 4, 104–107. https://doi.org/10.1016/S16722515(07)60247-4.

Graf, J.C., 1993. Lunar Soils Grain Size Catalog. NASA Reference Publication 1265.

He, C., Zeng, X., Wilkinson, A., 2013. Geotechnical Properties of GRC-3 Lunar Simulant. J. Aerosp. Eng. 26 (3).

Isachenkov, M., Chugunov, S., Landsman, Z., Akhatov, I., Metke, A., Tikhonov, A., Shishkovksy, I., 2022. Characterization of novel lunar highland and mare simulants for ISRU research applications. Icarus 376. https://doi.org/10.1016/j.icarus.2021.114873.

Kobrick, R.L., Budinski, K.G., Street, K.W.J., Klaus, D.M., 2010. Three-Body Abrasion Testing Using Lunar Dust Simulants to Evaluate Surface System Materials. Technical Memorandum TM2010-216781 NASA.

Landsman, Z.A., Schultz, C.D., Britt, D.T., Peppin, M., Kobrick, R.L., Metzger, P.T., Orlovskaya, N., 2021. Phobos regolith simulants PGI-1 and PCA-1. Adv. Space Res. 67, 3308–3327. https://doi.org/10.1016/j.asr.2021.01.024.

Long-Fox, J., Perman, J., Landsman, Z., Metke, A., Britt, D., 2022, Investigating the effects of composition on granular surface area: gas sorption analyses of high-fidelity lunar highlands and carbonaceous chondrite asteroid regolith simulants. In: 53rd Lunar and Planetary Science Conference, Houston, TX, USA, March 7-11, 2022.

Mankoc, C., Janda, A., Arévalo, R., Pastor, J.M., Zuriguel, I., Garcimartín, A., Maza, D., 2007. The flow rate of granular materials through an orifice. Granul. Matter 9, 407–414. https://doi.org/10.1007/s10035-007-0062-2.

McKay, D.S., Carter, J.L., Boles, W.W., Allen, C.C., Allton, J.H., 1994. JSC-1: A New Lunar Soil Simulant. Am. Soc. Civil Engineers Eng. Construct. Operations Space IV, 857–866.

Millwater, C., Long-Fox, J., Landsman, Z. Metke, A., Britt, D., 2022. Direct Shear Measurements of Lunar Regolith Simulants LHS-1, LHS-1D, LMS-1, and LMS-1D. In: Proceedings of the 53rd Lunar and Planetary Science Conference, Houston, TX, USA.

Oravec, H.A., Xeng, X., Asnani, V.M., 2010. Design and characterization of GRC-1: A soil for lunar terramechanics testing in Earth-ambient conditions. J. Terramech. 47 (6), 361–377.

Rickman, D., Street, K.W., 2008. Some expected mechanical characteristics of lunar dust: a geological view. AIP Conf. Proc. 969, 949. https://doi.org/10.1063/1.2845062.

Sibille, L., Carpenter, P., Schlagheck, R., French, R.A., 2006. Lunar Regolith Simulant Materials: Recommendations for Standardization, Production, and Usage. Technical Publication TP2006214605. NASA.

Schneider, C., Rasband, W., Eliceiri, K., 2012. NIH Image to ImageJ: 25 years of image analysis. Nat Methods 9, 671–675. https://doi.org/10.1038/nmeth.2089.

Simon, S.B., Papike, J.J., Laul, J.C., 1981. The lunar regolith: comparative studies of the Apollo and Luna sites. Petrology of soils from Apollo 17, Luna 16, 20, and 24. Lunar Planetary Sci. Conf. Proc. 12, 371–388.

Stoeser, D.B., Wilson, S.W., 2010. Design and specifications for the highland regolith prototype simulants NU-LHT-1M and -2M. NASA Tech. Rep., 2010–216438

Please cite this article as: J. M. Long-Fox, Z. A. Landsman, P. B. Easter et al., Geomechanical properties of lunar regolith simulants LHS-1 and LMS-1, Advances in Space Research, https://doi.org/10.1016/j.asr.2023.02.034